DNA Architectures

DOI: 10.1002/anie.201402437

Complex Reconfiguration of DNA Nanostructures**

Bryan Wei, Luvena L. Ong, Jeffrey Chen, Alexander S. Jaffe, and Peng Yin**

Abstract: *Nucleic acids have been used to create diverse synthetic structural and dynamic systems. Toehold-mediated strand displacement has enabled the construction of sophisticated circuits, motors, and molecular computers. Yet it remains challenging to demonstrate complex structural reconfiguration in which a structure changes from a starting shape to another arbitrarily prescribed shape. To address this challenge, we have developed a general structural-reconfiguration method that utilizes the modularly interconnected architecture of single-stranded DNA tile and brick structures. The removal of one component strand reveals a newly exposed toehold on a neighboring strand, thus enabling us to remove regions of connected component strands without the need to modify the strands with predesigned external toeholds. By using this method, we reconfigured a two-dimensional rectangular DNA canvas into diverse prescribed shapes. We also used this method to reconfigure a three-dimensional DNA cuboid.*

The self-assembly of nucleic acids (DNA and RNA) has produced diverse synthetic structures.[1–29] In particular, DNA origami[9,12–15,19,20,23] and single-stranded tiles (SSTs) and bricks[21,22,24,25] have enabled the construction of megadalton discrete structures with arbitrarily prescribed shapes. In parallel, researchers have used strand displacement to demonstrate the construction of dynamic systems,[30] such as switches,[31] walkers,[6,32,33] circuits,[34,32,35] and triggered assembly systems,[36,32] which can go through multiple states of different configurations, either in a directed or in an autonomous fashion.

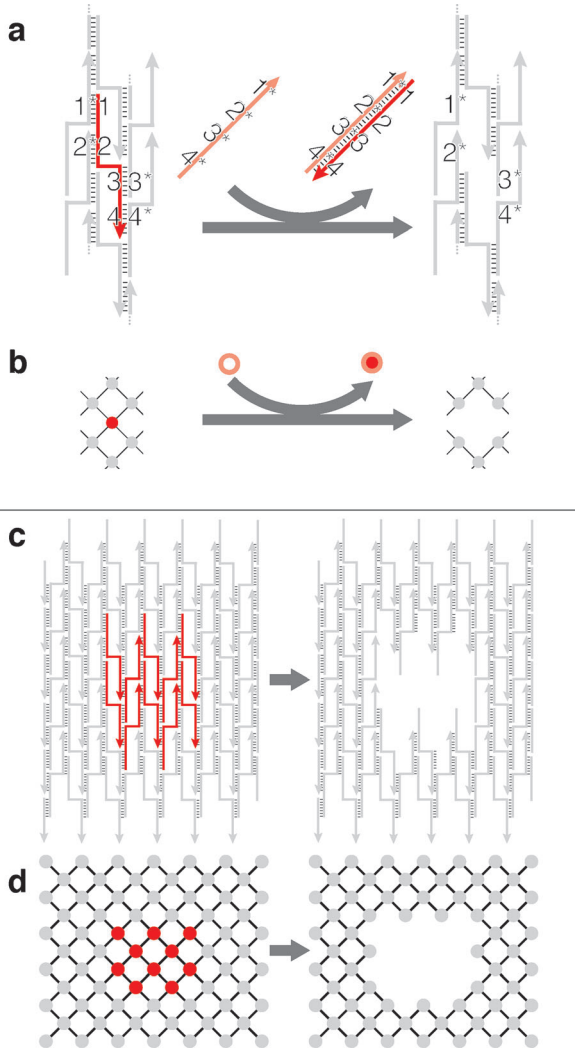

Figure 1. Schematic representation of structural reconfiguration from an SST canvas. a) Strand diagram of strand-displacement-based SST structural reconfiguration and b) the associated interaction graph. The strand/node to be displaced is highlighted in red with four domains 1, 2, 3, and 4 complementary to domains 1*, 2*, 3*, and 4*, respectively, of neighboring strands. When introduced into the system, a full complementary strand 4*–3*–2*–1* (in salmon) forms a duplex with the red target component strand to displace the target from the canvas. c) Strand diagram of strand displacement for an 12 helix (H) × 10 turns (T) canvas and d) the associated interaction graph. Strands/nodes highlighted in red on the left depict the subset of component strands to be displaced. The carved structure is shown on the right.

[*] Dr. B. Wei, L. L. Ong, J. Chen, A. S. Jaffe, Prof. Dr. P. Yin
Wyss Institute for Biologically Inspired Engineering
Harvard University, Boston, MA 02115 (USA)
E-mail: bryan.wei@wyss.harvard.edu
py@hms.harvard.edu
Homepage: http://molecular-systems.net
http://yin.hms.harvard.edu
Dr. B. Wei, Prof. Dr. P. Yin
Department of Systems Biology, Harvard Medical School
Boston, MA 02115 (USA)
L. L. Ong
Harvard-Massachusetts Institute of Technology (MIT)
Division of Health Sciences and Technology, MIT
Cambridge, MA 02139 (USA)

[**] We thank David Zhang and Yonggang Ke for discussions and Michelle K. Vhudzijena for technical assistance. This research is supported by an Office of Naval Research (ONR) Young Investigator Program Award (N000141110914), ONR grants (N000141010827, N000141310593), a National Science Foundation (NSF) Faculty Early Career Development Award (CCF1054898), an NSF Expedition in Computing Award (CCF1317291), NSF grants (CCF1162459, CMMI1333215), a National Institutes of Health (NIH) Director's New Innovator Award (1DP2OD007292), and a Wyss Institute for Biologically Inspired Engineering Faculty Startup Fund to P.Y. L.L.O. acknowledges support from the NSF through a Graduate Research Fellowship.

Supporting information for this article is available on the WWW under http://dx.doi.org/10.1002/anie.201402437.

Researchers have combined techniques for DNA strand displacement with methods for DNA structural assembly to create reconfigurable and/or reversible structures. For example, DNA origami boxes[13] and clamshells[20] were reconfigured from a closed to an open state through the toehold-mediated strand displacement of a few component strands in the structure. More complex reconfiguration methods have placed single-stranded toeholds at selected sites on the structure for shape transformation,[37–40] including the formation of a catenane derived from a DNA-origami Möbius strip[39] and the changing of fractal patterns in origami structures.[40]

However, it still remains challenging to develop a general framework for complex structural reconfiguration in which a structure changes from a particular starting shape to another arbitrarily prescribed shape. To address this challenge, we have developed a method based on the modularly interconnected architecture of single-stranded DNA tile and brick structures. The removal of one component strand reveals a newly exposed toehold on a neighboring strand, thus enabling us to remove connected regions of component strands without the need to modify them with predesigned external toeholds. This method applies only to SST/brick-based structures and not to origami-based structures because successful reconfiguration relies on the modular architecture.

By using this method, we demonstrate that a two-dimensional rectangular DNA SST canvas[21,25] can be reconfigured into many different shapes, including two full sets of the alphabet (one carved in intaglio, with the cavity forming the letters, and the other in relief, with DNA forming the letters). We also show that individual carved pieces can be reassembled to form the original canvas and be subjected to a second round of reconfigurations. Finally, this molecular-carving concept was also applied to a three-dimensional DNA-brick cuboid structure.[22] Overall, we demonstrate that SST and brick reconfiguration is a robust and modular method for engineering complex structural reconfiguration, with resolution at the scale of the component strand (e.g. 3×7 nm^2 for a typical 42 nt SST[21]).

In an SST structure,[21,25] each strand typically has four binding domains that are complementary to four different neighboring strands, as depicted in Figure 1 a,c. A self-assembled rectangular SST structure can be viewed as a "molecular canvas" and depicted as an interaction graph (Figure 1 b,d): each node represents a component strand, and each edge represents the binding interaction between two strands or nodes. A component strand (red) can be removed ("carving") by introducing a "carving strand" (salmon) that is fully complementary to the component strand (Figure 1 a,b). Unlike previous strand-displacement approaches, our method does not involve the use of an external toehold[31] (the detailed molecular mechanism is discussed later). By the displacement of multiple component strands with corresponding carving strands, the canvas can be reconfigured into a prescribed shape (Figure 1 c,d). Moreover, because each component strand can be removed modularly, it is possible to create a combinatorially large number of distinct shapes.

The canvas[25] was made by the self-assembly of 375 distinct component strands in 15 mM Mg^{2+} buffer at 48 °C overnight with 30 % yield, as determined by 2 % native gel electrophoresis (see Figure S4 in the Supporting Information). The structures showed the expected morphology and dimensions under atomic force microscopy (AFM) imaging (Figure 2 a, bottom left).

To reduce the overall time and potential human errors in the picking and mixing of carving strands, we wrote a computer program to design target shapes. The program takes the desired shape as input and then directs a robotic liquid handler to select the appropriate subset of strands from a master library of 375 carving strands. These carving strands were then applied to the canvas solution in an equimolar ratio for overnight incubation at 35 or 45 °C to produce the carved shapes. Figure 2 a shows an example of carving a corner off the canvas (the detailed carving mechanism is discussed later). Figure 2 b shows AFM images of the carved shapes of two full sets of the alphabet in intaglio and relief. The yield of the reconfigured structure in Figure 2 a was determined by gel electrophoresis to be 50 % (see Figure S17) and by AFM to be 99 % ($N = 202$; see Figure S30). Such a high AFM yield is not typical for the more complex alphabet structures that we carved (see Figures S4 and S5 (gels) and Figures S6–S15 (AFM images).

Unlike most previous strand-displacement-based dynamic systems, our carving scheme does not use predesigned external toeholds to initiate strand displacement. We thus conducted a set of experiments to study the effects of external

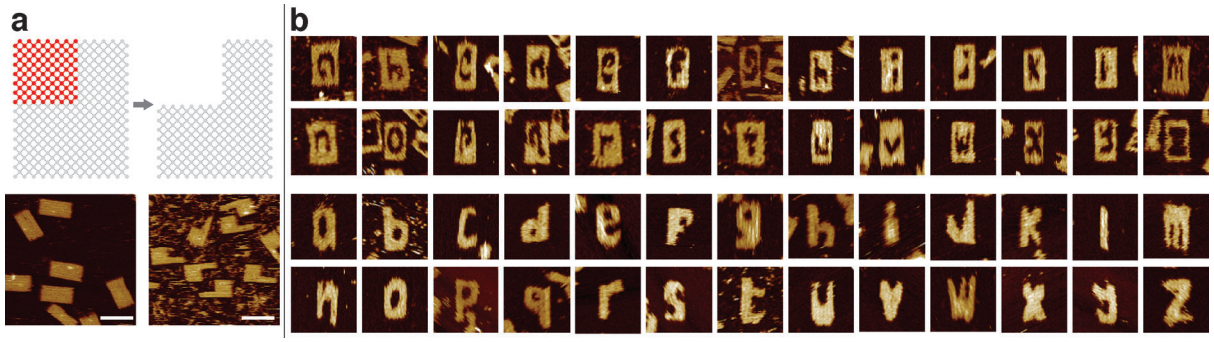

Figure 2. Alphabet sets reconfigured from a rectangular SST canvas. a) Interaction graphs (top) and AFM images (bottom) of the 24 H × 29 T canvas used in this study (left) and its reconfiguration into a rectangle with a missing corner (right). Scale bars: 100 nm. b) AFM images of letters of the alphabet carved in intaglio (top) and relief (bottom). Each image is 150×150 nm^2 in size. See Figures S4 and S5 in the Supporting Information for the results of agarose gel electrophoresis.

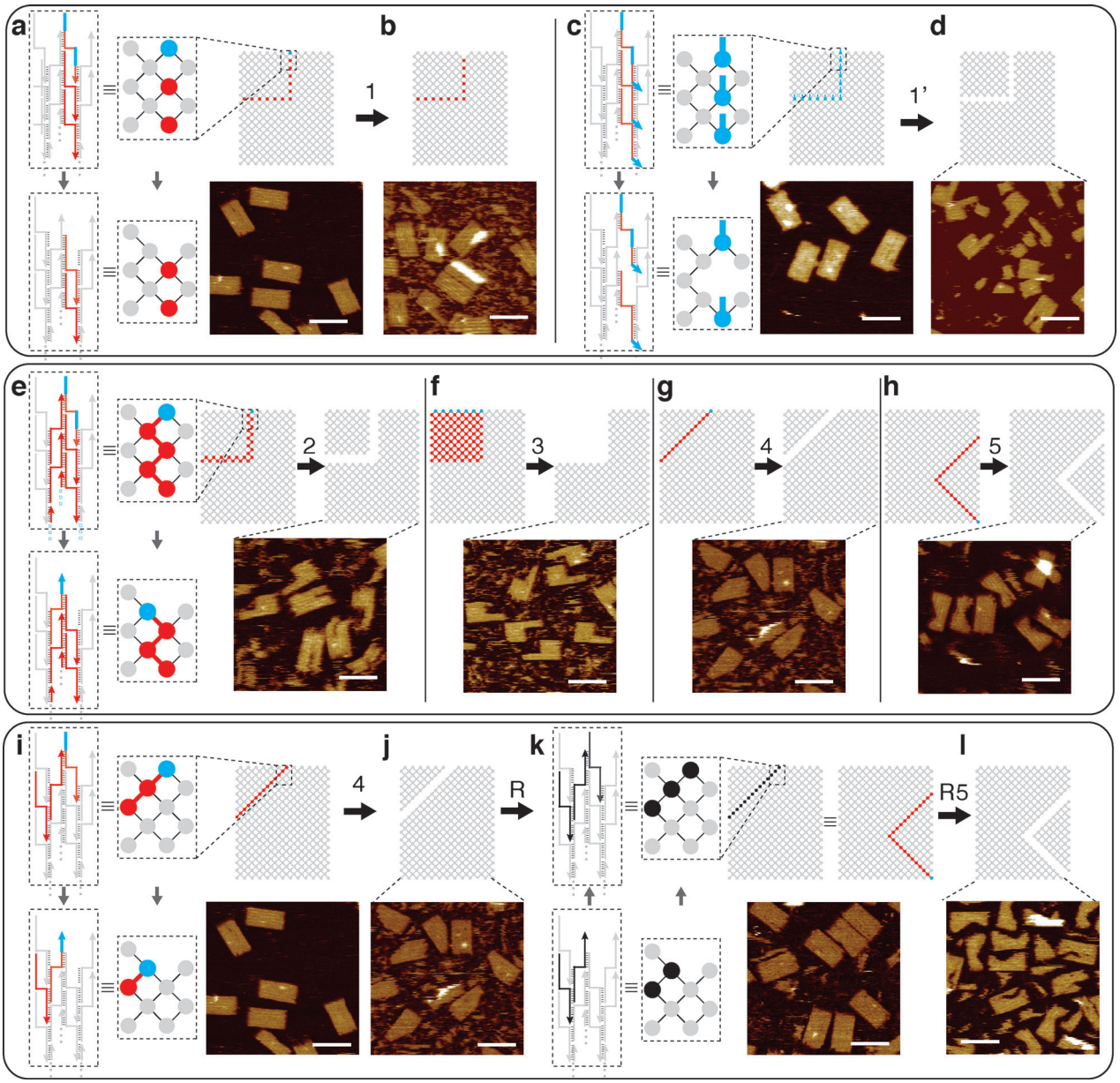

Figure 3. Diagrams and AFM images of a mechanistic study. In each case, interaction graphs with the carving pattern highlighted in red and blue are shown at the top, and AFM images are shown at the bottom (scale bars: 100 nm). a–d) Carving of pattern 1 without predesigned external toeholds (a, b) and pattern 1′ with predesigned external toeholds (c, d). e–h) Carving of patterns 2–5. i–l) Experiments demonstrating the reversibility of carving: reconfiguration of the canvas to give pattern 4, reassembly, and generation of pattern R5 (identical to pattern 5). The strand diagram and interaction graph boxed by the dashed lines show the reconfiguration mechanism at the zoomed-in fraction of the canvas (in a, c, e, i, and k). Gray depicts common components; red depicts the strands without external toeholds to be carved; blue marks the presence of an exposed single-stranded toehold; black indicates the introduction of strands for reassembly of the carved canvas pieces. See the Supporting Information for a detailed study of carving yields.

toeholds on carving (Figure 3a–d, patterns 1 and 1′ highlighted in red). We designed a different canvas in which the component strands in the carving pattern had external toeholds (blue; Figure 3c,d, pattern 1′). After overnight carving at 45 °C, gel electrophoresis showed minimal carving for the toehold-free canvas (Figure 3a,b, pattern 1; yield around 0%; see Figure S16) but significant carving for the canvas with external toeholds (Figure 3c,d; 19–39% yield; see Figure S16). AFM images were consistent with the gel results: carving a canvas without predesigned external toeholds rarely reached completion (ca. 14% yield; see Figure S27), whereas carving a canvas with external toeholds led to higher conversion (ca. 81% yield; see Figure S28). The observation of higher AFM yields than gel yields suggests that partially carved structures may have comigrated with the intact canvas on the gel, but may have broken apart under AFM (e.g. during the deposition or imaging process).

We next designed a second set of experiments to test five distinct connection patterns of component strands to be carved (carving patterns) in a canvas without external toeholds. The carving samples ([carving strands]/[component

strands]: 1:1, 2:1, or 3:1) from patterns 1–5 were incubated at 45 °C overnight before agarose gel electrophoresis and AFM imaging. When the sample from carving pattern 1 was compared with those from patterns 2–5, significantly lower carving yields were observed for pattern 1 by gel electrophoresis and AFM (see the Supporting Information for a detailed yield study).

A component strand to be carved is denoted by a red or blue node. A blue node indicates the presence of an unpaired single-stranded domain. Each node in carving pattern 1 (Figure 3a,b) is disjoint from any other node in the pattern. In contrast, in each of patterns 2–5 (Figure 3e–h), the nodes to be carved are fully connected, such that a path consisting only of nodes to be carved exists between any two nodes within the carving pattern. Additionally, each of these patterns contains at least one blue node representing a component strand at the end of a constituent helix with exposed poly-T domain(s) that can serve as an external toehold (Figure 3e–h).

The above experiments on the carving patterns demonstrate that appending an external toehold on each individual node in a carving pattern composed of disjoint nodes can enable effective carving (e.g. pattern 1′) of an initially hard-to-carve pattern (e.g. pattern 1). In contrast, effective carving can be obtained in a fully connected carving pattern (e.g. patterns 2–5) composed mostly of toehold-free nodes if the pattern also contains an initial blue node (e.g. the strand with an exposed poly-T domain at the helix end). In the latter case, the carving reaction can be initiated from an external toehold in a blue node, and followed by a cascade of sequential exposure of initially hidden toeholds. Detailed schematics of this mechanism can be found in the zoomed-in diagrams of Figure 3e,i. For example, in the zoomed-in diagrams of Figure 3e, the strand with initial toeholds of poly-T domains (top, shown as a blue node and as blue domains in the strand diagram) can be displaced by a carving strand. The displacement of this strand will reveal a newly exposed toehold on its neighboring strand (bottom, shown as a blue node and as a blue domain in the strand diagram), allowing this neighbor to be displaced next. Following this mechanism, a cascade of new toeholds will be sequentially generated, enabling the removal of all strands in the carving pattern. Note that such a consecutive toehold exposure is not possible in the disjoint pattern (e.g. pattern 1, see zoom-in of Figure 3a). In the case of carving pattern 1′, where each node contains a predesigned external toehold, each components can be displaced independently in parallel (zoom-in of Figure 3b).

In the cases of the intaglio alphabet and the cavities in the relief set where the carving patterns contain no initial external toehold, the cascading could be initiated from the transient dissociation of a few bases on an internal component, or an unpaired domain from empty neighboring components (such a defect rate is estimated as 5–10 % for a certain component in a DNA origami structure.[41]

We tested the reversibility of this structural reconfiguration by adding back the displaced components following the carving of pattern 4 (Figure 3j,k, pattern R). This overnight reaction at 45 °C was sufficient to glue back the two carved out pieces almost seamlessly with a yield of around 89 % by gel electrophoresis and 78 % by AFM (Figure 3k; see Figures S18 and S33). The reassembled canvases were then subjected to a second round of carving (pattern R5; Figure 3l), which resulted in yields similar to those obtained directly from carving the original canvas (gel yield of 58 % and AFM yield of 72 %; Figures S18 and S34).

We then applied this carving method to 3D DNA-brick cuboids. By using a 10 helix × 10 helix × 80 base-pair structure (Figure 4a, top) that we reported previously,[22] we tested multiple carving patterns. We used a reaction temperature (28 °C) lower than that for the 2D carving, since 3D structures contain 8 nt binding domains and are less thermally stable than the 2D structures, which contain 10 or 11 nt binding domains. The successful results of carving a corner off (Figure 4b, top) or a tunnel through a cuboid (Figure 4c, top) and carving the cuboid into two halves (Figure 4d, top) were shown by agarose gel electrophoresis (see Figure S37) and transmission electron microscopy (TEM; Figure 4, bottom). Because of the limited thermal stability and the limited accessibility of the majority of the component strands, the structural reconfiguration of 3D DNA structures is much more difficult than that of the 2D counterparts, and it is even more challenging to obtain fine features. Since it is difficult to find a temperature high enough for fast strand displacement but low enough (< 30 °C) to maintain structural stability, we

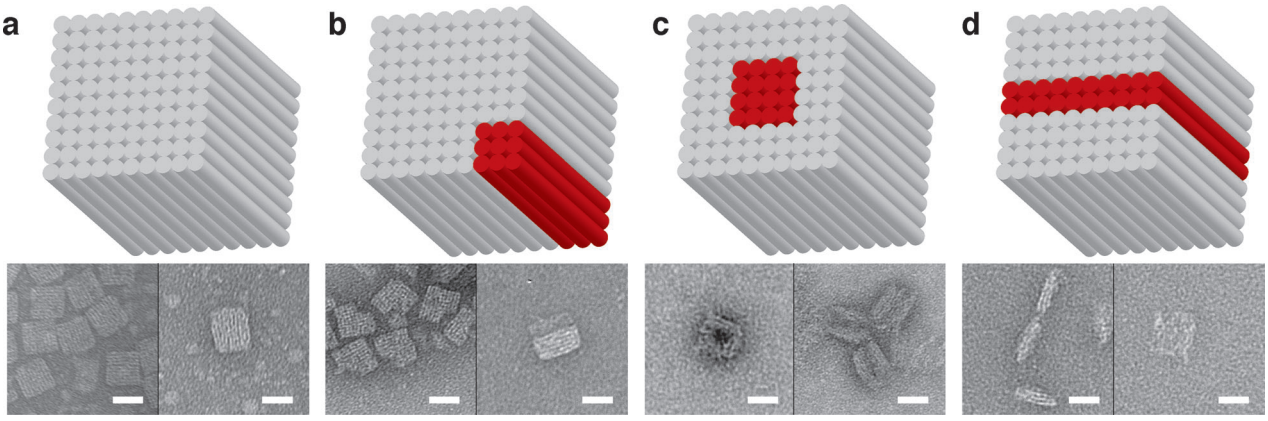

Figure 4. Structural reconfiguration from a 3D cuboid. Top: cylinder model of the cuboid (red cylinders denote those to be displaced); bottom: TEM images (scale bars: 20 nm). a) Cuboid before structural reconfiguration. b) Carving of a corner from the cuboid. c) Carving of a tunnel through the cuboid. d) Carving of the cuboid into two halves.

were only able to demonstrate a few cases of successful carving with coarse resolution.

Carving may not appear to be thermodynamically favorable, since a component strand in the canvas structure that is fully paired with its neighbors has the same designed number of hybridized bases as when it is bound to its fully complementary carving strand (after carving). However, the carving off of a component strand may help to alleviate the electrostatic repulsion that results from the closely packed neighboring DNA duplexes in the canvas structure[9,21] and release the mechanical stress that might be accrued at the cross-over points,[42] thereby favoring the reaction.

In a similar way to typical toehold-mediated strand-displacement circuits, our carving system shows leakage (carving can be initiated in a connected region even when no external toehold is present), which we utilize to initiate carving. However, it is conceivable that under other reaction conditions (e.g. if the carving reaction is carried out at room temperature over a shorter period of time rather than at an elevated temperature (35–45 °C) overnight as in this study), such leakage could be mitigated, and carving may only start at a site with an external toehold. Such a system would be analogous to a strand-displacement circuit embedded in a nanostructure (the canvas), in which case the strand-displacement cascade would be directly coupled with the structural change at single-strand resolution. This system would provide a platform to explore the rich interplay between structure, dynamics, and computation. For example, it would be interesting to design spatial logic gates and circuits: A multi-input AND gate could be designed as a carving path with the component strands along the path serving as the inputs and the strand at the end of the path serving as the output, or a two-input OR gate could be designed as two converging paths with one strand on each path serving as the inputs and the strand at the merging point serving as the output. In the latter case, when multiple strands along each path are used as inputs, these two converging paths would together implement a disjunctive normal form formula ($[A_1$ AND A_2 AND … AND $A_m]$ OR $[B_1$ AND B_2 AND … AND $B_n]$).

Received: February 14, 2014
Revised: March 22, 2014
Published online: June 4, 2014

Keywords: DNA bricks · nanostructures · single-stranded tiles · strand displacement · structural reconfiguration

[1] N. C. Seeman, *J. Theor. Biol.* **1982**, *99*, 237–247.
[2] J. Chen, N. C. Seeman, *Nature* **1991**, *350*, 631–633.
[3] T. J. Fu, N. C. Seeman, *Biochemistry* **1993**, *32*, 3211–3220.
[4] E. Winfree, F. Liu, L. A. Wenzler, N. C. Seeman, *Nature* **1998**, *394*, 539–544.
[5] H. Yan, S. H. Park, G. Finkelstein, J. H. Reif, T. H. LaBean, *Science* **2003**, *301*, 1882–1884.
[6] W. B. Sherman, N. C. Seeman, *Nano Lett.* **2004**, *4*, 1203–1207.
[7] A. Chworos, I. Severcan, A. Y. Koyfman, P. Weinkam, E. Oroudjev, H. G. Hansma, L. Jaeger, *Science* **2004**, *306*, 2068–2072.
[8] S. H. Park, C. Pistol, S. J. Ahn, J. H. Reif, A. R. Lebeck, C. Dwyer, T. H. Labean, *Angew. Chem.* **2006**, *118*, 749–753; *Angew. Chem. Int. Ed.* **2006**, *45*, 735–739.
[9] P. W. K. Rothemund, *Nature* **2006**, *440*, 297–302.
[10] Y. He, T. Ye, M. Su, C. Zhang, A. E. Ribbe, W. Jiang, C. Mao, *Nature* **2008**, *452*, 198–201.
[11] P. Yin, R. Hariadi, S. Sahu, H. M. T. Choi, S. H. Park, T. H. LaBean, J. H. Reif, *Science* **2008**, *321*, 824–826.
[12] Y. Ke, J. Sharma, M. Liu, K. Jahn, Y. Liu, H. Yan, *Nano Lett.* **2009**, *9*, 2445–2447.
[13] E. S. Andersen, M. Dong, M. M. Nielsen, K. Jahn, R. Subramani, W. Mamdouh, M. M. Golas, B. Sander, H. Stark, C. L. P. Oliveira, J. S. Pedersen, V. Birkedal, F. Besenbacher, K. V. Gothelf, J. Kjems, *Nature* **2009**, *459*, 73–76.
[14] S. M. Douglas, H. Dietz, T. Liedl, B. Högberg, F. Graf, W. M. Shih, *Nature* **2009**, *459*, 414–418.
[15] H. Dietz, S. M. Douglas, W. M. Shih, *Science* **2009**, *325*, 725–730.
[16] J. Zheng, J. J. Birktoft, Y. Chen, T. Wang, R. J. Sha, P. E. Constantinou, S. L. Ginell, C. Mao, N. C. Seeman, *Nature* **2009**, *461*, 74–77.
[17] I. Severcan, C. Geary, A. Chworos, N. Voss, E. Jacovetty, L. Jaeger, *Nat. Chem.* **2010**, *2*, 772–779.
[18] C. J. Delebecque, A. B. Lindner, P. A. Silver, F. A. Aldaye, *Science* **2011**, *333*, 470–474.
[19] D. Han, S. Pal, J. Nangreave, Z. Deng, Y. Liu, H. Yan, *Science* **2011**, *332*, 342–346.
[20] S. M. Douglas, I. Bachelet, G. M. Church, *Science* **2012**, *335*, 831–834.
[21] B. Wei, M. Dai, P. Yin, *Nature* **2012**, *485*, 623–626.
[22] Y. Ke, L. L. Ong, W. M. Shih, P. Yin, *Science* **2012**, *338*, 1177–1183.
[23] D. Han, S. Pal, Y. Yang, S. Jiang, J. Nangreave, Y. Liu, H. Yan, *Science* **2013**, *339*, 1412–1415.
[24] C. Myhrvold, M. Dai, P. A. Silver, P. Yin, *Nano Lett.* **2013**, *13*, 4242–4248.
[25] B. Wei, M. Dai, C. Myhrvold, Y. Ke, R. Jungmann, P. Yin, *J. Am. Chem. Soc.* **2013**, *135*, 18080–18088.
[26] C. Lin, Y. Liu, S. Rinker, H. Yan, *ChemPhysChem* **2006**, *7*, 1641–1647.
[27] W. M. Shih, C. Lin, *Curr. Opin. Struct. Biol.* **2010**, *20*, 276–282.
[28] N. B. Leontis, A. Lescoute, E. Westhof, *Curr. Opin. Struct. Biol.* **2006**, *16*, 279–287.
[29] N. C. Seeman, *Annu. Rev. Biochem.* **2010**, *79*, 65–87.
[30] D. Y. Zhang, G. Seelig, *Nat. Chem.* **2011**, *3*, 103–113.
[31] B. Yurke, A. J. Turberfield, A. P. Mills, F. C. Simmel, J. L. Neumann, *Nature* **2000**, *406*, 605–608.
[32] P. Yin, H. M. T. Choi, C. R. Calvert, N. A. Pierce, *Nature* **2008**, *451*, 318–322.
[33] T. Omabegho, R. Sha, N. C. Seeman, *Science* **2009**, *324*, 67–71.
[34] G. Seelig, D. Soloveichik, D. Y. Zhang, E. Winfree, *Science* **2006**, *314*, 1585–1588.
[35] L. Qian, E. Winfree, *Science* **2011**, *332*, 1196–1201.
[36] R. M. Dirks, N. A. Pierce, *Proc. Natl. Acad. Sci. USA* **2004**, *101*, 15275–15278.
[37] H. Yan, X. Zhang, Z. Shen, N. C. Seeman, *Nature* **2002**, *415*, 62–65.
[38] Z. Li, Y. Ke, C. Lin, H. Yan, Y. Liu, *Chem. Commun.* **2008**, 4318–4320.
[39] D. Han, S. Pal, Y. Liu, H. Yan, *Nat. Nanotechnol.* **2010**, *5*, 712–717.
[40] F. Zhang, J. Nangreave, Y. Liu, H. Yan, *Nano Lett.* **2012**, *12*, 3290–3295.
[41] R. Jungmann, C. Steinhauer, M. Scheible, A. Kuzyk, P. Tinnefeld, F. C. Simmel, *Nano Lett.* **2010**, *10*, 4756–4761.
[42] P. K. Maiti, T. A. Pascal, N. Vaidehi, W. A. Goddard, *Nucleic Acids Res.* **2004**, *32*, 6047–6056.

